

**Comparative Fluxome and Metabolome Analysis of Formate as an Auxiliary Substrate for Penicillin Production in Glucose-Limited Cultivation of *Penicillium chrysogenum***

Wang, Guan; Wang, Xinxin; Wang, Tong; van Gulik, Walter; Noorman, Henk J.; Zhuang, Yingping; Chu, Ju; Zhang, Siliang

**DOI**

[10.1002/biot.201900009](https://doi.org/10.1002/biot.201900009)

**Publication date**

2019

**Document Version**

Final published version

**Published in**

Biotechnology Journal

**Citation (APA)**

Wang, G., Wang, X., Wang, T., van Gulik, W., Noorman, H. J., Zhuang, Y., Chu, J., & Zhang, S. (2019). Comparative Fluxome and Metabolome Analysis of Formate as an Auxiliary Substrate for Penicillin Production in Glucose-Limited Cultivation of *Penicillium chrysogenum*. *Biotechnology Journal*, 14(10), Article 1900009. <https://doi.org/10.1002/biot.201900009>

**Important note**

To cite this publication, please use the final published version (if applicable). Please check the document version above.

**Copyright**

Other than for strictly personal use, it is not permitted to download, forward or distribute the text or part of it, without the consent of the author(s) and/or copyright holder(s), unless the work is under an open content license such as Creative Commons.

**Takedown policy**

Please contact us and provide details if you believe this document breaches copyrights. We will remove access to the work immediately and investigate your claim.

# Comparative Fluxome and Metabolome Analysis of Formate as an Auxiliary Substrate for Penicillin Production in Glucose-Limited Cultivation of *Penicillium chrysogenum*

Guan Wang, Xinxin Wang, Tong Wang, Walter van Gulik, Henk J. Noorman, Yingping Zhuang,\* Ju Chu,\* and Siliang Zhang

During glucose-limited growth, a substantial input of adenosine triphosphate (ATP) is required for the production of  $\beta$ -lactams by the filamentous fungus *Penicillium chrysogenum*. Formate dehydrogenase has been confirmed in *P. chrysogenum* for formate oxidation allowing an extra supply of ATP, and coassimilation of glucose and formate has the potential to increase penicillin production and biomass yield. In this study, the steady-state metabolite levels and fluxes in response to cofeeding of formate as an auxiliary substrate in glucose-limited chemostat cultures at the dilution rates ( $D$ ) of both  $0.03\text{ h}^{-1}$  and  $0.05\text{ h}^{-1}$  are determined to evaluate the quantitative impact on the physiology of a high-yielding *P. chrysogenum* strain. It is observed that an equimolar addition of formate is conducive to an increase in both biomass yield and penicillin production at  $D = 0.03\text{ h}^{-1}$ , while this is not the case at  $D = 0.05\text{ h}^{-1}$ . In addition, a higher cytosolic redox status ( $\text{NADH}/\text{NAD}^+$ ), a higher intracellular glucose level, and lower penicillin productivity are only observed upon formate addition at  $D = 0.05\text{ h}^{-1}$ , which are virtually absent at  $D = 0.03\text{ h}^{-1}$ . In conclusion, the results demonstrate that the effect of formate as an auxiliary substrate on penicillin productivity in the glucose-limited chemostat cultivations of *P. chrysogenum* is not only dependent on the formate/glucose ratio as published before but also on the specific growth rate. The results also imply that the overall process productivity and quality regarding the use of formate should be further explored in an actual industrial-scale scenario.

## 1. Introduction


The filamentous fungus *Penicillium chrysogenum* is an industrially relevant workhorse for the production of  $\beta$ -lactam antibiotics, such as penicillin G (PenG) and penicillin V, and for the production of intermediates such as 6-aminopenicillanic acid (6-APA) and 7-aminodeacetoxycephalosporanic acid (7-ADCA).<sup>[1]</sup> Major improvements have been achieved in productivity through random mutagenesis and screening, and, nowadays, “omics” diagnostic tools and directed metabolic engineering as well as process analytical technology (PAT). Still, *P. chrysogenum* holds potential for further improvement since the current yield is still far from reaching the theoretical limits.<sup>[2]</sup> Among these “omics” approaches, the metabolome covers all metabolites in an organism, which is governed by cellular-regulatory processes sensitive to genetic and/or environmental perturbations.<sup>[3,4]</sup> Comparative metabolomics approaches can provide insights into cellular metabolism by providing a comprehensive analysis of all metabolites in a biological system and can reveal

Dr. G. Wang, X. Wang, T. Wang, Prof. Y. Zhuang, Prof. J. Chu, Prof. S. Zhang  
State Key Laboratory of Bioreactor Engineering  
East China University of Science and Technology (ECUST)  
130 Meilong Road  
Shanghai 200237, P. R. China  
E-mail: ypzhuang@ecust.edu.cn; juchu@ecust.edu.cn

Prof. W. van Gulik  
Cell Systems Engineering  
Department of Biotechnology  
Delft University of Technology  
Delft, The Netherlands

Prof. H. J. Noorman  
DSM Biotechnology Center  
Delft, The Netherlands

Prof. H. J. Noorman  
Department of Biotechnology  
Delft University of Technology  
Delft, The Netherlands

 The ORCID identification number(s) for the author(s) of this article can be found under <https://doi.org/10.1002/biot.201900009>.

DOI: 10.1002/biot.201900009

metabolic relationships and metabolite responses.<sup>[5–11]</sup> In addition, complementary to metabolite concentrations, it also provides an opportunity for linking metabolites and their pathways.<sup>[4,12]</sup> As an example, a metabolome study investigating the steady-state relation between central metabolism, amino acid biosynthesis, and penicillin production in *P. chrysogenum* revealed that the penicillin production flux is mostly influenced by the availability of energy and redox cofactors.<sup>[13]</sup>

It has been concluded that substantial amounts of adenosine triphosphate (ATP) (73 mol of ATP per mole of penicillin G) are required from primary metabolism during penicillin production,<sup>[14]</sup> and this additional ATP drain was later reported to be mainly caused by futile cycling of the precursor phenylacetic acid (PAA); PAA passively diffuses into the cell and at the same time is actively exported outside the cell for detoxification at the expense of ATP.<sup>[15]</sup> During glucose-limited growth, this reduces the product yield with respect to glucose utilization. To exacerbate this, to the best of our knowledge, in a large-scale industrial penicillin fermentation process, due to the addition of the highly concentrated substrate at a single inlet point, the cells are repeatedly subjected to oscillating substrate concentrations.<sup>[16]</sup> Consequently, the impact of these oscillations on the cells in most cases gives rise to a reduction in either yield, titer, or productivity, or combinations thereof and an increase of the by-product formation.<sup>[17,18]</sup> This can be anticipated because multilayered regulatory mechanisms at the expense of extra ATP and/or reducing equivalents are required for transients and tradeoffs of phenotypic switching in a fluctuating limited environment.<sup>[19,20]</sup> In recent scale-down studies, de Jonge et al.<sup>[21]</sup> and Wang et al.<sup>[22]</sup> imposed repetitive glucose pulses on glucose-limited chemostat cultures of *P. chrysogenum*, revealing that periodic glucose availability that translates to glucose gradients as experienced by the cells on a large-scale vessel resulted in a performance loss, i.e., reduced biomass-specific penicillin formation rate ( $q_{\text{PenG}}$ ). The timescales of these experiments are relevant to actual fed-batch processes. Therefore, these datasets allow for a prediction of full-scale reality. Tang et al.<sup>[23]</sup> recently published a 9-pool metabolic structured model for biomass growth and penicillin production under dynamic situations and this model was then integrated with a computational fluid dynamics (CFD) model, which indicated that yield losses observed at the laboratory-scale were very likely operative in large-scale systems, and the predictions of the combined model in a fed-batch process did match the development of  $q_{\text{PenG}}$  in time in an industrial fed-batch.<sup>[24]</sup> This combined model also showed that in a 54 m<sup>3</sup> penicillin fermentor, *P. chrysogenum* exhibited dynamic fluctuations in the biomass-specific growth rate ( $\mu$ ) to respond to variations in extracellular glucose levels in different parts of the fermentor.<sup>[24]</sup> Furthermore, previous glucose-limited chemostat cultivations by van Gulik et al.,<sup>[25]</sup> covering a wide range of dilution rates for the *P. chrysogenum* strain, have shown that  $q_{\text{PenG}}$  is highly dependent on  $\mu$ , and also both the 9-pool metabolic model outputs and the experimental results by Tang et al.<sup>[23]</sup> have shown that extracellular, intracellular, and  $q$ -rate profiles would be in a dynamic concert with alternating glucose feast/famine conditions and feed-ramp

conditions, where  $\mu$  linearly decreased from 0.05 h<sup>-1</sup> to 0.005 h<sup>-1</sup> in 100 h after the achievement of steady state.

Auxiliary substrates can be simultaneously utilized as an extra energy source to increase the yield on the carbon source. Ideally, compounds such as formate or thiosulfate, which are inexpensive sources of reducing power and/or free energy, have been used in previous studies, and this “auxiliary substrate” concept has presented an interesting approach to reduce the costs of industrial fermentation.<sup>[26,27]</sup> Although the current bioproduct formation via C1 carbon assimilation is not as efficient as that using conventional carbon sources, the use of methane,<sup>[28]</sup> methanol,<sup>[29]</sup> formic acid,<sup>[30]</sup> and carbon dioxide<sup>[31]</sup> is on the rise.<sup>[32,33]</sup> Particularly, formic acid is an attractive auxiliary carbon source for the bio-based production of chemicals as it can be efficiently derived from the C1 gas such as CO<sub>2</sub>, CH<sub>4</sub>, and CO by microbial gas fermentation.<sup>[34,35]</sup> Formate has been used as a suitable auxiliary substrate for yeasts and fungi as many of these organisms contain an nicotinamide adenine dinucleotide (NADH)-linked formate dehydrogenase (EC 1.2.1.1; FDH) that catalyzes the oxidation of formate to CO<sub>2</sub> but cannot assimilate formate.<sup>[26]</sup> Application of metabolic engineering tools efficaciously makes it possible to extend the scope of substrate utilization for micro-organisms, which are not capable of expressing related enzymes. In *Escherichia coli* (*E. coli*), this NADH-linked FDH was heterologously introduced to induce a shift to fermentation even in the presence of oxygen and favored the production of more reduced metabolites, which was evidenced by a dramatic increase in the ethanol:acetate ratio.<sup>[36]</sup> The recent pioneering work by the Sang Yup Lee and colleagues reported that in *E. coli* strains, assimilation of both formic acid and CO<sub>2</sub> was achieved through the reconstructed tetrahydrofolate cycle and the reverse glycine cleavage pathway.<sup>[30]</sup> In *Mannheimia succiniciproducens*, fed-batch fermentations showed that formic acid can be efficiently utilized through systems metabolic engineering as a secondary carbon source to increase the yield and productivity of succinic acid.<sup>[37]</sup> In anaerobic *Saccharomyces cerevisiae* (*S. cerevisiae*) cultures, the glycerol yield was further enhanced through overexpression of FDH and glycerol-3-phosphate dehydrogenase.<sup>[38]</sup> In *P. chrysogenum*, FDH has been confirmed as a cytosolic NAD<sup>+</sup>-dependent enzyme, and cofeeding formate with glucose within a proper range of formate:glucose ratios ( $\leq 4.5$  mole mole<sup>-1</sup>) increased the yield of both biomass and penicillin on glucose at the low growth rate of 0.03 h<sup>-1</sup>.<sup>[39]</sup> However, little information with respect to changes in metabolite levels and fluxomics due to the addition of formate as the auxiliary substrate during penicillin production has been reported.

In the present work, the effect of formate as the auxiliary substrate for penicillin production under glucose-limited cultivation of *P. chrysogenum* was revisited through a comparative steady-state metabolomics and fluxomics study. *P. chrysogenum* chemostat cultivation at a dilution rate of 0.03 h<sup>-1</sup> was carried out not only for comparison with earlier experiments,<sup>[39]</sup> but for direct comparison with continuous cultivation at the higher dilution rate of 0.05 h<sup>-1</sup>. This is more related to the earlier experiments for the *P. chrysogenum* strain studied and also keeps experiments more practical in terms of residence times needed for the achievement of steady state.

## 2. Experimental Section

### 2.1. Strain and Medium

In all experiments, a high-producing *P. chrysogenum* strain, DS17690, was used; the characteristics of this strain have been extensively studied and reported.<sup>[13,22,25,40]</sup> The strain was kindly donated by DSM Sinochem Pharmaceuticals (Delft, The Netherlands) as spores on rice grains.

Chemostat cultivation ( $D = 0.03 \text{ h}^{-1}$ ): The medium for both batch and chemostat cultivation contained the same components (per kilogram of demineralized water): 8.25 g glucose monohydrate, 3.5 g  $(\text{NH}_4)_2\text{SO}_4$ , 0.8 g  $\text{KH}_2\text{PO}_4$ , 0.5 g  $\text{MgSO}_4 \cdot 7\text{H}_2\text{O}$ , and 2 mL of a trace element solution.

Chemostat cultivation ( $D = 0.05 \text{ h}^{-1}$ ): The medium for both batch and chemostat cultivation contained the same components (per kilogram of demineralized water): 16.5 g glucose monohydrate, 5 g  $(\text{NH}_4)_2\text{SO}_4$ , 1 g  $\text{KH}_2\text{PO}_4$ , 0.5 g  $\text{MgSO}_4 \cdot 7\text{H}_2\text{O}$ , and 2 mL of a trace element solution.

The trace element solution contained (per kilogram of demineralized water) 75 g  $\text{Na}_2\text{EDTA} \cdot 2\text{H}_2\text{O}$ , 10 g  $\text{ZnSO}_4 \cdot 7\text{H}_2\text{O}$ , 10 g  $\text{MnSO}_4 \cdot \text{H}_2\text{O}$ , 20 g  $\text{FeSO}_4 \cdot 7\text{H}_2\text{O}$ , 2.5 g  $\text{CaCl}_2 \cdot 2\text{H}_2\text{O}$ , and 2.5 g  $\text{CuSO}_4 \cdot 5\text{H}_2\text{O}$ . In addition, the media contained the following amounts of PAA per kilogram: 0.408 g batch medium and 0.681 g chemostat medium.

Relative to the controlled chemostat cultivation with glucose as the sole carbon source, in the experimental runs, an equal molar amount of formic acid was added. The preparation and sterilization of the cultivation medium as well as the inoculation procedure have been described previously.<sup>[41]</sup>

### 2.2. Chemostat Cultivation

Bioreactor setup and process control in all chemostat cultivations were the same as reported previously.<sup>[42]</sup> Briefly, after glucose depletion in the batch phase, aerobic glucose-limited chemostat cultures (pH 6.5, 25 °C,  $2 \text{ L min}^{-1}$ , 400 rpm) of 3 L working volume were carried out in a 5 L turbine stirred bioreactor (Shanghai Guoqiang Bioengineering Equipment Co. Ltd., China). Samples for both intracellular and extracellular metabolite level analysis were rapidly taken during each residence time throughout the whole cultivation process.

### 2.3. Sampling for the Determination of Cell Dry Weight (CDW) and Total Organic Carbon (TOC)

An amount of 15 mL broth was withdrawn and divided into three portions for the measurement of CDW using glass fiber filters (47 mm in diameter, 1  $\mu\text{m}$  pore size, type A/E; Pall Corporation, East Hills, NY, USA) predried overnight at 70 °C. For a CDW sample, 5 mL of the broth was filtered, and the cell cake was washed twice with 10 mL of demineralized water and dried at 70 °C for 24 h. The biomass-containing filters were cooled to room temperature in a desiccator before weighing. Another 10 mL of the broth and 10 mL of the supernatant were stored at  $-20 \text{ °C}$  for analysis of the TOC concentration in the

broth and in the supernatant with a TOC analyzer (TOC-5050A; Shimadzu).

### 2.4. Rapid Sampling and Quenching for Analysis of Extracellular Glucose and Other Excreted Metabolites

The cold steel-bead method combined with liquid nitrogen was efficiently used for fast filtration and quenching of extracellular enzyme activities.<sup>[21,43]</sup> About 32 g of stainless-steel beads (4 mm diameter) was stored in a syringe and precooled to  $-20 \text{ °C}$ . Approximately 1 mL of the broth was transferred from the bioreactor into the syringe for cooling of the sample within a fraction of a second to close to  $0 \text{ °C}$  and was then rapidly filtered through a Millex HV 0.45  $\mu\text{m}$  filter (Millipore, Billerica, MA, USA). For the absolute determination of extracellular metabolites, 2  $\mu\text{L}$  of 100 mM *N*-ethylmaleimide (NEM) for thiol group protection<sup>[44]</sup> and 20  $\mu\text{L}$  of  $\text{U-}^{13}\text{C}$ -labeled cell extract<sup>[45,46]</sup> as an internal standard (IS) were added before the filtrate sample was quickly frozen in liquid nitrogen. Subsequently the sample was stored at  $-80 \text{ °C}$  until analysis.

### 2.5. Rapid Sampling, Quenching, and Subsequent Extraction for Analysis of Intracellular Metabolites

A well-established rapid sampling, quenching, and subsequent extraction protocol for the determination of intracellular metabolites was used to acquire the true snapshots of the cellular conditions. In this study, this protocol was exactly followed as described in Wang et al.<sup>[47]</sup>

### 2.6. Analytical Techniques

Samples for metabolites quantification were analyzed using gas chromatography–mass spectrometry (GC–MS) (7890A GC coupled to 5975C MSD; Agilent Technologies, Santa Clara, CA, USA) and liquid chromatography–tandem mass spectrometry (LC–MS/MS) (DIONEX Ultimate 3000 UPLC system coupled to a TSQ QUANTUM ULTRA mass spectrometer; ThermoFisher Scientific, San Jose, USA). Extracellular glucose, other excreted sugar polyols and intracellular metabolites of the glycolytic pathway, the tricarboxylic acid (TCA) cycle, and the pentose phosphate (PP) pathway were quantified by GC–MS using the isotope dilution mass spectrometry (IDMS) method, as described previously.<sup>[21,46,48]</sup> The concentrations of the nucleotides and penicillin pathway-related metabolites were also analyzed with the IDMS method; details of the applied LC–electrospray ionization (ESI)–MS/MS procedure have been described elsewhere.<sup>[49,50]</sup>

The concentrations of PAA and PenG in the filtrate were determined by an isocratic reversed-phase high-performance liquid chromatography (HPLC) method. Samples were analyzed by an HPLC (Agilent 1100; Agilent Technologies) equipped with an Agilent Zorbax SB-C18 reversed-phase column (150 mm  $\times$  4.6 mm ID, 5  $\mu\text{m}$ ). The sample injection volume was 5  $\mu\text{L}$ . The detection wavelength was set at 214 nm. The flow rate was

1.5 mL min<sup>-1</sup>. The column temperature was maintained at 25 °C. The mobile phase consisted of 0.44 g KH<sub>2</sub>PO<sub>4</sub> per liter in the elution (65% water and 35% acetonitrile [v/v]). Formate was analyzed by the HPLC equipped with a Metacarb H Plus column (300 mm × 7.8 mm; Varian Inc., Palo Alto, CA, USA) at 50 °C. Samples were isocratically eluted with 5 mM H<sub>2</sub>SO<sub>4</sub> at 0.4 mL min<sup>-1</sup> and detected by a UV detector at 210 nm. Organic carbon in the total broth (TOC<sub>broth</sub>) and the filtrate (TOC<sub>supernatant</sub>) was analyzed by a TOC analyzer (TOC-5050A; Shimadzu) according to the manufacturers' instructions.

## 2.7. Calculation Procedures

The biomass-specific rates were calculated from the respective broth and gas-phase compound balances and then the obtained conversion rates were reconciled using the approach of Verheijen.<sup>[51]</sup>

## 2.8. Flux Balance Analysis

The RAVEN toolbox (Reconstruction, Analysis, and Visualization of Metabolic Networks) is an open-access software package (<http://biomet-toolbox.chalmers.se/index.php?page=downtools-raven>), where the latest version of a genome-scale model for *P. chrysogenum* strain can be accessed. In this study, a genome-scale metabolic model (GEM), which comprises 1471 unique biochemical reactions and 1006 open reading frames for *P. chrysogenum* Wisconsin 54-1255 strain, was used to estimate the metabolic flux distribution of the strains under the studied conditions.<sup>[52]</sup>

## 2.9. Goeman's Global Test

A global test for metabolic pathway differences between the two conditions was conducted according to Hendrickx et al.<sup>[53]</sup>

## 3. Results and Discussion

### 3.1. Uptake/Secretion Rates

In all chemostat runs, after three to five residence times, the steady state could be reached with the observation that time patterns of CDW (Figure 1), and the O<sub>2</sub> and CO<sub>2</sub> fractions in the offgas did not significantly change (data not shown). The CDW, reconciled biomass-specific rates, and relevant yields on glucose, and the corresponding carbon and degree of reduction recoveries from two different carbon-limited chemostat cultures are shown in Table 1. The carbon and redox balances were found to be close to satisfactory for all chemostat runs, suggesting negligible by-product formation. Compared to the reference steady-state conditions at the dilution rates of 0.03 h<sup>-1</sup> and 0.05 h<sup>-1</sup>, the biomass concentrations were about 2.2-fold and 7% higher in the dual substrate-limited chemostat culture (Table 1). Due to the addition of the auxiliary substrate, formate, the respiratory quotient (RQ) was 23% and 14% higher at values of 1.28 and 1.22, respectively, which were close to the theoretical

values (1.21 and 1.18) calculated by assuming that no free energy input is required for formate transport into the cell.<sup>[39]</sup>

Notably, the cell lysis rate, which was characterized by the other excreted organic carbon rate, was about 60% and 35% lower in the dual substrate-limited conditions at the dilution rate of 0.03 h<sup>-1</sup> and 0.05 h<sup>-1</sup>, respectively, compared to the glucose-limited conditions. Possibly, under the same dilution rate, the cell lysis rate is reduced under the dual substrate-limited conditions in which more energy can be produced with the catabolism of formate. In both conditions, consistent with previous studies,<sup>[13,54]</sup> over 90% of the PAA was converted into the PenG, accompanied by the formation of a small amount of benzylpenicilloic acid (PIO) and ortho-hydroxy-PAA (o-OH-PAA) (data not shown), indicating that there is only marginal catabolism of PAA in this high-yielding strain.

The time-resolved measurements of PAA, biomass, PenG concentration, and the  $q_{\text{PenG}}$  profiles are shown in Figure 1. It was observed that  $q_{\text{PenG}}$  reached a maximum value at about 75–80 h and 120–130 h after the start-up of the chemostat cultivation under both conditions (Figure 1D), which indicates the time duration needed for the induction of penicillin pathway enzymes.<sup>[41]</sup> It has been shown that cointegration of the C<sub>1</sub> compound formate can increase penicillin production and biomass yield at a growth rate of 0.03 h<sup>-1</sup> within proper formate:glucose ratios.<sup>[39]</sup> In this study, the results at  $D = 0.03 \text{ h}^{-1}$  were consistent with the previous finding, showing the increased biomass yield and thus increased penicillin production with the same maximum  $q_{\text{PenG}}$  (Table 1). However, in contrast with this finding, the supply of the auxiliary substrate under glucose-limited chemostat cultivation at a growth rate of 0.05 h<sup>-1</sup> did not contribute to the increase of the biomass yield and the penicillin productivity; rather, the specific penicillin production rate was 27% lower after 250 h of chemostat cultivation (Table 1). In addition, with the addition of formic acid as the auxiliary substrate in both conditions, the time durations required for reaching their maximum  $q_{\text{PenG}}$  values were prolonged. This might have been caused by either glucose repression (Figure 5F) or formic acid inhibition (Figure 2) or combinations thereof.

In acetone–butanol–ethanol fermentation by *Clostridium acetobutylicum*, it has been observed that the addition of 1 mM formic acid triggered the “acid crash” and resulted in a decrease of the solvent production, and assimilation of formic acid by the expression of heterologous FDH can relieve this “acid crash” phenomenon.<sup>[55]</sup> In fed-batch cultures of *Ralstonia eutropha* on formic acid, Grunwald et al.<sup>[56]</sup> observed that there was a linear decrease in the biomass yield with the increasing residual formic acid concentration (0 → 33 mM). As shown in Figure 2, the residual formate concentration maintained values of 8 mM and 3 mM after about 100 h and 75 h of chemostat cultivations, indicating that time was required for the full induction of FDH in this high-yielding *P. chrysogenum* strain, respectively. At dilution rates of 0.03 h<sup>-1</sup> and 0.05 h<sup>-1</sup>, the expected expression periods ( $3 \times (1/D)$ ) of a protein were about 100 h and 60 h, respectively, in agreement with the observed time length in the fluctuating formic acid concentration. However, the residual formic acid concentration remained at a higher value at  $D = 0.03 \text{ h}^{-1}$  than at  $D = 0.05 \text{ h}^{-1}$  (Figure 2). Also, Table 1 shows that formic acid was taken up by the cells more

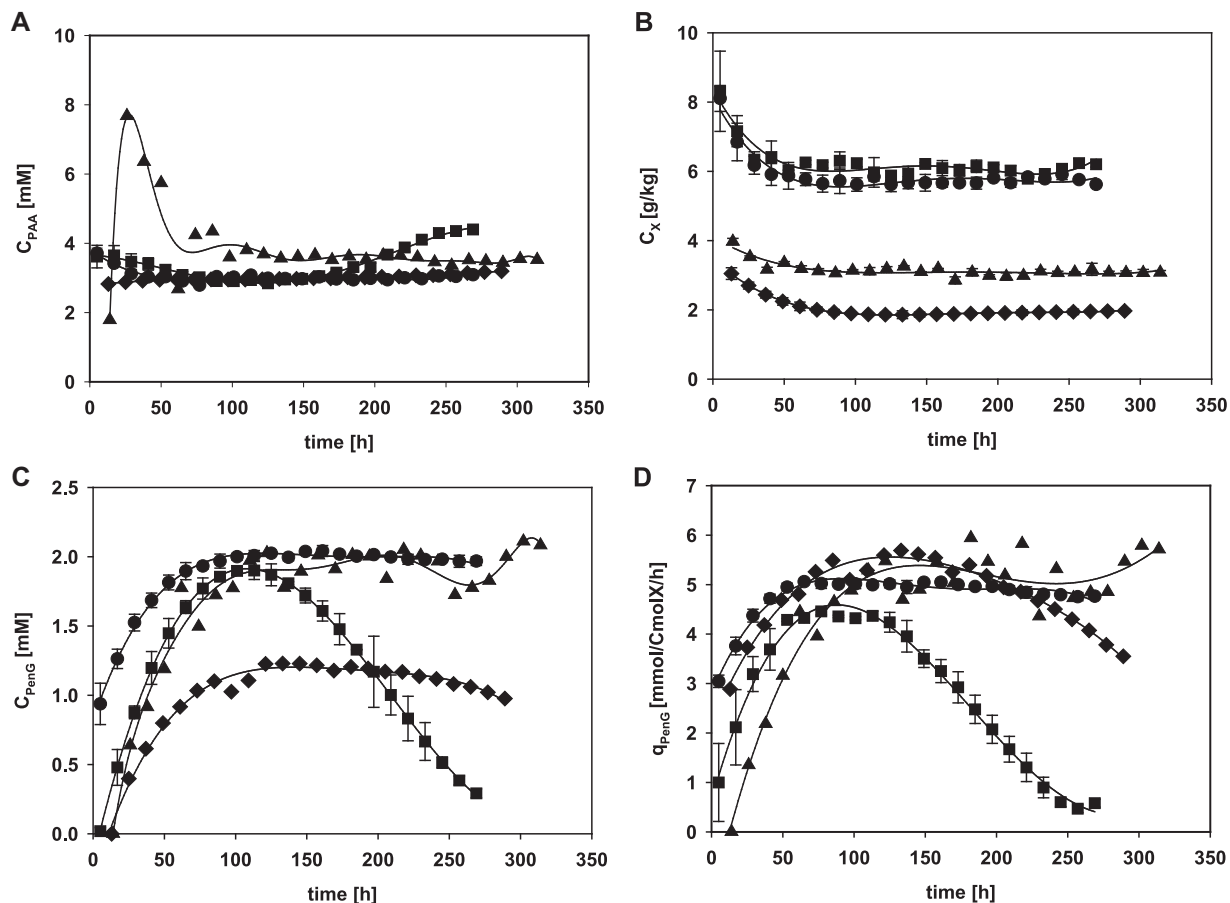


**Figure 1.** Measured concentrations of PAA, biomass, PenG, and the biomass-specific PenG production rate ( $q_{\text{PenG}}$ ) during carbon-limited chemostat cultivation under two different conditions. A) PAA concentration, B) biomass concentration, C) PenG concentration, and D) biomass-specific PenG production rate. The glucose-limited chemostat culture ( $\bullet$ ,  $0.05 \text{ h}^{-1}$ ;  $\blacklozenge$ ,  $0.03 \text{ h}^{-1}$ ); the dual substrate-limited chemostat culture ( $\blacksquare$ ,  $0.05 \text{ h}^{-1}$ ;  $\blacktriangle$ ,  $0.03 \text{ h}^{-1}$ ). Measurements are given as the average  $\pm$  standard deviation of at least three technical replicates. Time zero signifies the start-up of the chemostat cultivations. The solid curves show the trend lines of the experimental data within the observation time.

efficiently at a higher  $\mu$  of  $0.05 \text{ h}^{-1}$  compared to  $0.03 \text{ h}^{-1}$ . This might result in the accumulation of intracellular formic acid, which, surpassing a certain threshold concentration, might lead to weak acid uncoupling and inhibit the penicillin biosynthetic pathways. However, this should be further confirmed in the following experiments through a) determination of intracellular formic acid concentration and b) increase of FDH activity.

### 3.2. Distribution of Intracellular Fluxes

A previously developed genome-scale model of the parental *P. chrysogenum* strain was used to map the flux distribution under the two carbon-limited chemostat cultivations.<sup>[52]</sup> An energy-independent mechanism was reported to be responsible for formate transport in *P. chrysogenum*.<sup>[39]</sup> Under the dual substrate-limited chemostat culture, 1 mol of formate was oxidized via the cytosolic  $\text{NAD}^+$ -dependent FDH to form 1 mol of  $\text{CO}_2$ , 1 mol of water, and 1 mol of NADH. The fluxes through central carbon metabolism and towards the biosynthesis of the penicillin precursors alpha amino adipic acid (AAA), cysteine (Cys), and

valine (Val) for these two conditions are shown (Figure 3). At a dilution rate of  $0.03 \text{ h}^{-1}$ , the results show that in the observed time range (100–250 h), the fluxes are not significantly changed (Figure 3A,B). However, notably, 26% and 10% more fluxes through the mitochondrial isocitrate dehydrogenase-dependent reaction in the TCA cycle might be associated with the higher demand of nicotinamide adenine dinucleotide phosphate (NADPH) for the higher penicillin productivity in the glucose-limited conditions at the dilution rates of  $0.03 \text{ h}^{-1}$  and  $0.05 \text{ h}^{-1}$ , respectively. Also, after 100 h of chemostat cultivation at the dilution rates of  $0.05 \text{ h}^{-1}$ , compared with the glucose-limited conditions, about 12% lower fluxes were observed in the glycolytic pathway. The reduction in the glycolytic pathway flux at  $D = 0.05 \text{ h}^{-1}$  may be caused by several reasons: a) a lower specific glucose uptake rate: this will directly reduce the flux towards the glycolytic pathway since the flux through the PP pathway and the TCA cycle were not significantly changed; b) formate uptake is energetically more favorable than glucose uptake. As reported in Hariss et al.,<sup>[39]</sup> formate can passively diffuse into the cell without the expense of ATP, while the uptake of glucose and thus glucose consumption in the upper part of the glycolysis need an ATP

**Table 1.** Comparison of the reconciled biomass-specific rates and relevant yields of *P. chrysogenum* strains on glucose obtained from carbon-limited cultures grown at dilution rates of 0.03 h<sup>-1</sup> and 0.05 h<sup>-1</sup> after 100 h and 250 h of chemostat cultivation under two different conditions.

	Glucose-limited <i>D</i> = 0.03 h <sup>-1</sup>		Glucose-limited <i>D</i> = 0.05 h <sup>-1</sup>		Dual substrate-limited <i>D</i> = 0.03 h <sup>-1</sup>		Dual substrate-limited <i>D</i> = 0.05 h <sup>-1</sup>	
	100 h	250 h	100 h	250 h	100 h	250 h	100 h	250 h
<i>C<sub>X</sub></i> [g kg <sup>-1</sup> ]	1.88 ± 0.01	1.93 ± 0.05	5.69 ± 0.22	5.84 ± 0.12	3.14 ± 0.02	3.09 ± 0.01	6.17 ± 0.18	6.16 ± 0.12
<i>μ<sub>actual</sub></i> [mCmolX CmoleX <sup>-1</sup> h <sup>-1</sup> ]	34.18 ± 1.29	33.30 ± 1.29	65.32 ± 0.29	63.42 ± 0.72	32.95 ± 1.53	32.73 ± 1.53	58.93 ± 3.15	59.83 ± 3.10
<i>q<sub>s, glucose</sub></i> <sup>a)</sup> [mmol CmoleX <sup>-1</sup> h <sup>-1</sup> ]	-15.12 ± 0.39	13.98 ± 0.42	-21.43 ± 0.63	-19.99 ± 0.29	-13.33 ± 0.47	-13.44 ± 0.48	-19.35 ± 0.99	-18.76 ± 0.92
<i>q<sub>s, formate</sub></i> <sup>a)</sup> [mmol CmoleX <sup>-1</sup> h <sup>-1</sup> ]	—	—	—	—	-9.28 ± 0.93	-9.33 ± 0.94	-18.91 ± 0.98	-18.51 ± 0.92
<i>q<sub>O<sub>2</sub></sub></i> a) [mmol CmoleX <sup>-1</sup> h <sup>-1</sup> ]	-50.60 ± 1.70	-44.78 ± 1.90	-55.58 ± 3.10	-52.45 ± 1.30	-40.76 ± 2.20	-41.63 ± 2.20	-60.02 ± 2.80	-55.79 ± 2.10
<i>q<sub>CO<sub>2</sub></sub></i> a) [mmol CmoleX <sup>-1</sup> h <sup>-1</sup> ]	52.94 ± 1.70	47.07 ± 1.90	59.45 ± 3.10	56.02 ± 1.30	52.39 ± 2.30	53.30 ± 2.30	72.93 ± 3.00	68.43 ± 2.20
<i>q<sub>other excreted organic carbon</sub></i> <sup>a),b)</sup> [mmol CmoleX <sup>-1</sup> h <sup>-1</sup> ]	3.81 ± 0.48	3.62 ± 0.46	15.32 ± 0.66	13.42 ± 0.46	2.28 ± 0.30	2.30 ± 0.30	8.93 ± 0.56	9.83 ± 0.30
<i>q<sub>PAA</sub></i> <sup>a)</sup> [mmol CmoleX <sup>-1</sup> h <sup>-1</sup> ]	-0.52 ± 0.03	-0.50 ± 0.03	-0.51 ± 0.02	-0.48 ± 0.01	-0.56 ± 0.05	-0.56 ± 0.05	-0.48 ± 0.05	-0.34 ± 0.05
<i>q<sub>PenG</sub></i> <sup>a)</sup> [mmol CmoleX <sup>-1</sup> h <sup>-1</sup> ]	0.48 ± 0.03	0.47 ± 0.02	0.49 ± 0.02	0.45 ± 0.01	0.53 ± 0.04	0.53 ± 0.05	0.43 ± 0.03	0.33 ± 0.02
<i>Y<sub>X/S, glucose</sub></i> <sup>a)</sup> [CmolX molS <sup>-1</sup> ]	2.01 ± 0.06	2.12 ± 0.06	3.17 ± 0.02	3.17 ± 0.03	2.30 ± 0.08	2.26 ± 0.08	3.05 ± 0.05	3.19 ± 0.05
<i>Y<sub>O/S, glucose</sub></i> <sup>a)</sup> [mol mol <sup>-1</sup> ]	3.35 ± 0.07	3.20 ± 0.10	2.59 ± 0.12	2.62 ± 0.05	3.06 ± 0.12	3.10 ± 0.12	3.10 ± 0.07	2.97 ± 0.09
Carbon recovery [%]	99.92 ± 2.21	100.01 ± 2.57	98.32 ± 0.76	96.78 ± 1.17	100.09 ± 2.73	100.06 ± 2.70	95.42 ± 3.02	95.90 ± 2.71
<i>γ</i> balance [%]	98.40 ± 1.00	98.61 ± 0.90	103.48 ± 0.18	101.66 ± 0.28	89.46 ± 0.99	89.33 ± 0.98	99.16 ± 0.74	99.01 ± 0.68

Glucose-limited, only glucose as the carbon source; dual substrate-limited, both glucose and formic acid as the carbon source. Measurements are given as the average ± standard deviation of at least two technical duplicates.

<sup>a)</sup>The molar weight of 28.05 gDW Cmole<sup>-1</sup> was assumed for the calculation.<sup>[21]</sup>

<sup>b)</sup>The rate of excreted carbon is quantified as *q<sub>other excreted organic carbon</sub>*, which is measured from the TOC measurements. *μ<sub>actual</sub>* = *D*(dilution rate) + *q<sub>other excreted organic carbon</sub>*, assuming that all other excreted organic carbon arises from cell lysis.

investment; c) the regulation of the cytosolic redox environment: in dual substrate-limited chemostat cultures, the oxidation of formate resulted in the formation of NADH, which significantly increased the cytosolic NADH/NAD<sup>+</sup> ratio. In *S. cerevisiae*, it has been observed that a higher NADH/NAD<sup>+</sup> ratio renders the

glycolytic pathway less thermodynamically feasible and to some extent inhibits the glucose uptake.<sup>[57]</sup> Combined with the results in the current study, it can be extrapolated that a change in the cytosolic redox status leading to a change in thermodynamic force and glucose uptake also applies to *P. chrysogenum*. Another observation at *D* = 0.05 h<sup>-1</sup> is that the fluxes through the mitochondrial isocitrate dehydrogenase-dependent reaction became comparable under the substrate-limited conditions, and an approximately 11% higher flux through the rest of the TCA cycle was observed in the dual substrate-limited conditions after 250 h of chemostat cultivation. This indicated that there may be a stronger inhibition of the TCA cycle by the highly increased cytosolic NADH/NAD<sup>+</sup> ratio upon the catabolism of formate in the first 100 h of chemostat cultivation; however, *P. chrysogenum* was gradually adapted to balance the cytosolic redox status, which was manifested by the gradual decrease of the cytosolic NADH/NAD<sup>+</sup> ratio (Figure 4A). Evidence for this change in the flux through the glycolytic pathway and the TCA cycle can further be obtained by comparing mass action ratios (MARs) of near-equilibrium reactions in central metabolism. The MAR for PEP/(2 + 3PG) in the dual substrate-limited conditions (0.71) was significantly higher than in the glucose-limited conditions (0.06), which substantiated the reduction in glycolytic flux in the dual substrate-limited conditions. Further, the MAR for malate/fumarate in the dual substrate-limited conditions was gradually decreased (2.6 → 2.2) in the time range of 100–220 h of chemostat cultivation, which promoted the gradual adaption of the redox status. Interestingly, this change in the redox status is not reflected

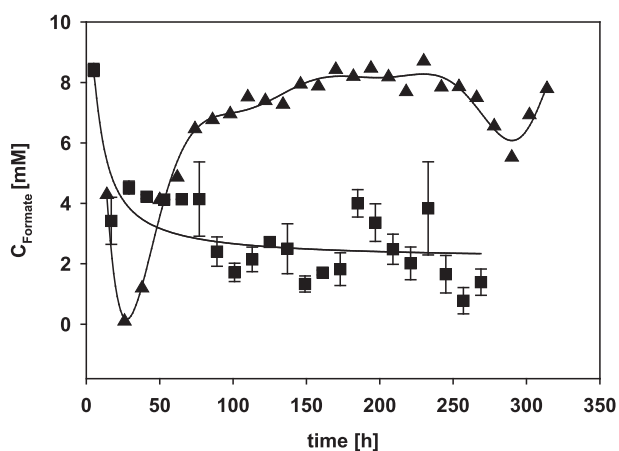


**Figure 2.** Measured concentrations of formate during the dual substrate-limited chemostat culture (■, 0.05 h<sup>-1</sup>; ▲, 0.03 h<sup>-1</sup>). Measurements are given as the average ± standard deviation of at least three technical replicates. Time zero signifies the start-up of the chemostat cultivations. The solid curves show the trend lines of the experimental data within the observation time.

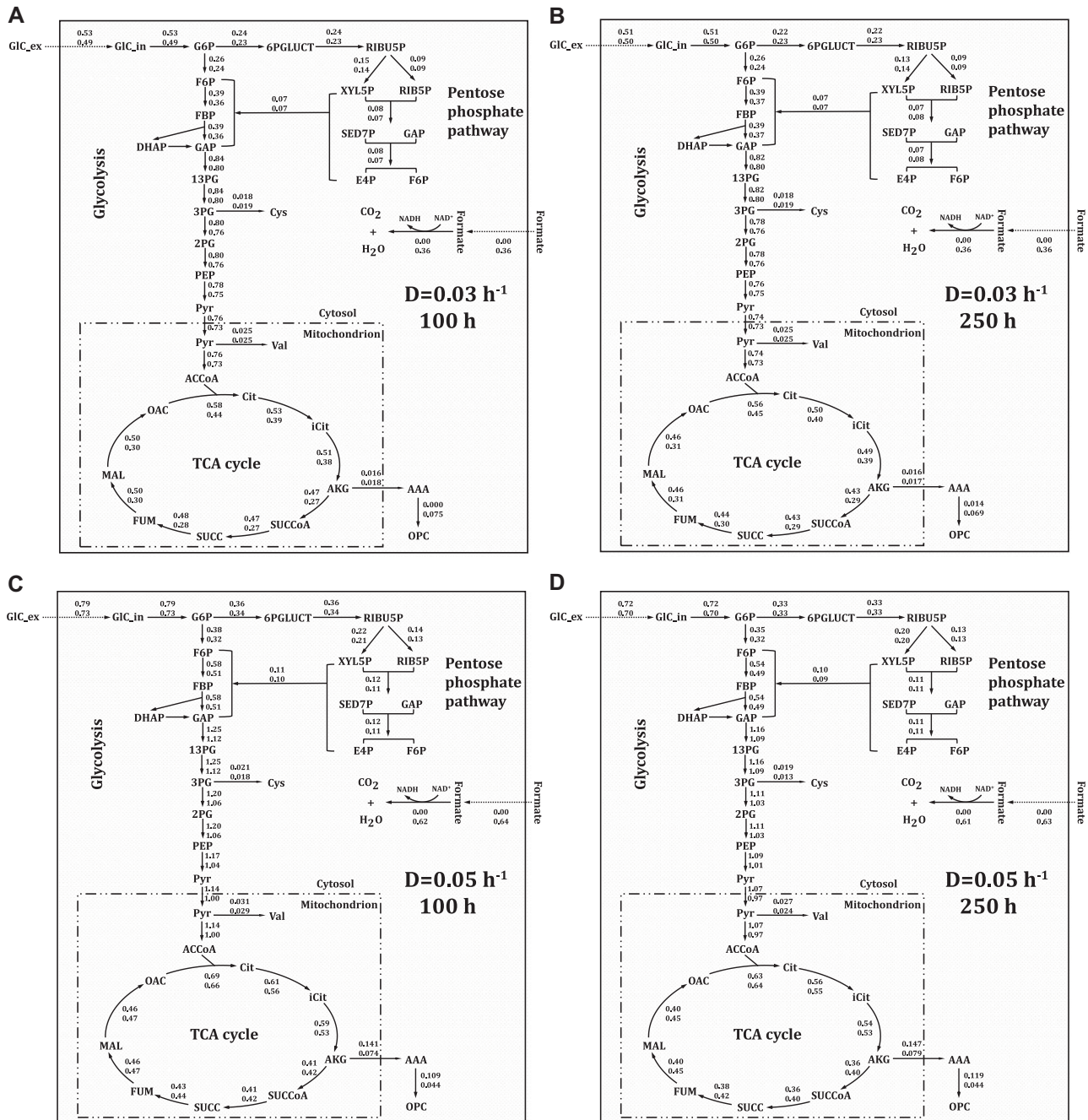


**Figure 3.** Calculated fluxes (in  $\text{mmol gDW}^{-1} \text{h}^{-1}$ ) through the central metabolic pathways of *P. chrysogenum* from the previously established genome-scale model<sup>[52]</sup> after 100 h (left panel) and 250 h (right panel) of chemostat cultivation at dilution rates of both  $0.03 \text{ h}^{-1}$  and  $0.05 \text{ h}^{-1}$  under the two conditions. Specific rates in Table 1 were used as the model input, and maximization of the growth rate was set as the objective function. The direction of the arrow indicates the direction of the flux. The upper and lower numbers represent the flux distribution in glucose-limited and dual substrate-limited chemostat cultures, respectively.

in the dual substrate-limited condition with  $D = 0.03 \text{ h}^{-1}$  (Figure 4A), which might be ascribed to the lower specific formic acid consumption rate (Table 1).

Compared with the glucose-limited chemostat conditions at  $D = 0.05 \text{ h}^{-1}$ , the biosynthetic fluxes towards AAA were decreased about twofold, while the fluxes towards Cys (14–32%) and Val (6–10%) were decreased from 100 h to 250 h

of chemostat cultivation in the dual substrate-limited chemostat cultures (Figure 3C,D). The reduction in fluxes leading to these precursor amino acids might be associated with the 12–27% lower specific penicillin production rate in this time duration. There may be several reasons for the significant reduction in the flux leading to AAA under the dual substrate-limited chemostat cultivation: 1) the reduced flux needed for the penicillin



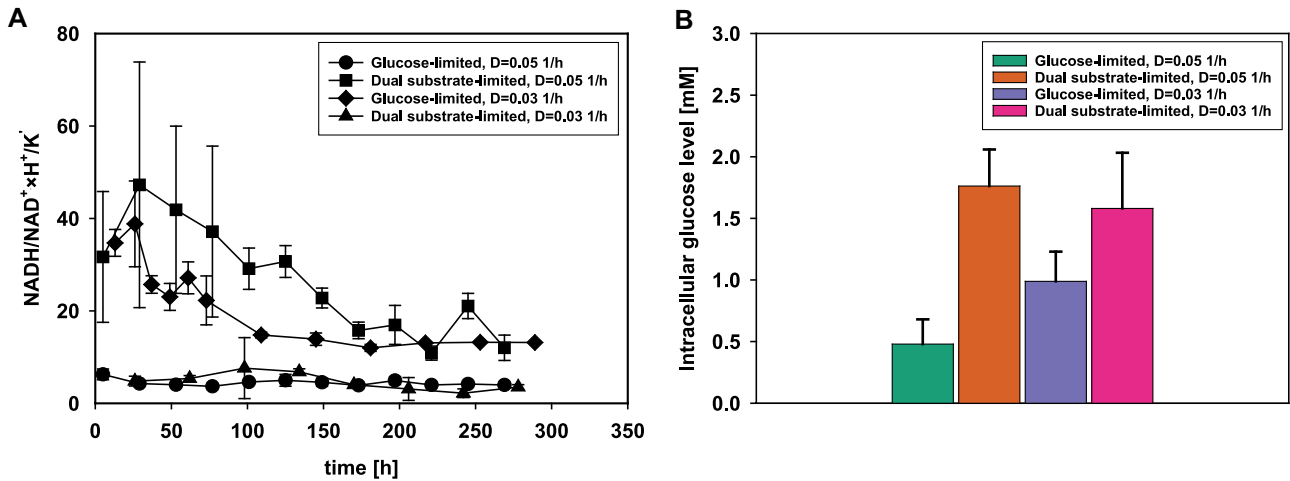


**Figure 4.** A) Calculated cytosolic-free NADH/NAD<sup>+</sup> ratio, assuming constant intracellular pH and *K'*. The glucose-limited chemostat culture (●, 0.05 h<sup>-1</sup>; ◆, 0.03 h<sup>-1</sup>); the dual substrate-limited chemostat culture (■, 0.05 h<sup>-1</sup>; ▲, 0.03 h<sup>-1</sup>). Time zero signifies the start-up of the chemostat cultivations. B) Intracellular glucose concentrations. An intracellular volume of 2.5 mL gDCW<sup>-1</sup> is assumed for the conversion.

productivity; 2) the reduced spontaneous conversion of AAA into the by-product 6-oxopiperidine-2-carboxylic acid (OPC). According to the simulation results at *D* = 0.05 h<sup>-1</sup>, the predicted OPC excretion rates were about three times higher in the glucose-

limited condition than in the dual substrate-limited condition (Figure 3C,D). From an economic point of view, it is interesting to note that in the dual substrate-limited conditions not only was the formation of PenG reduced but also that of the by-product

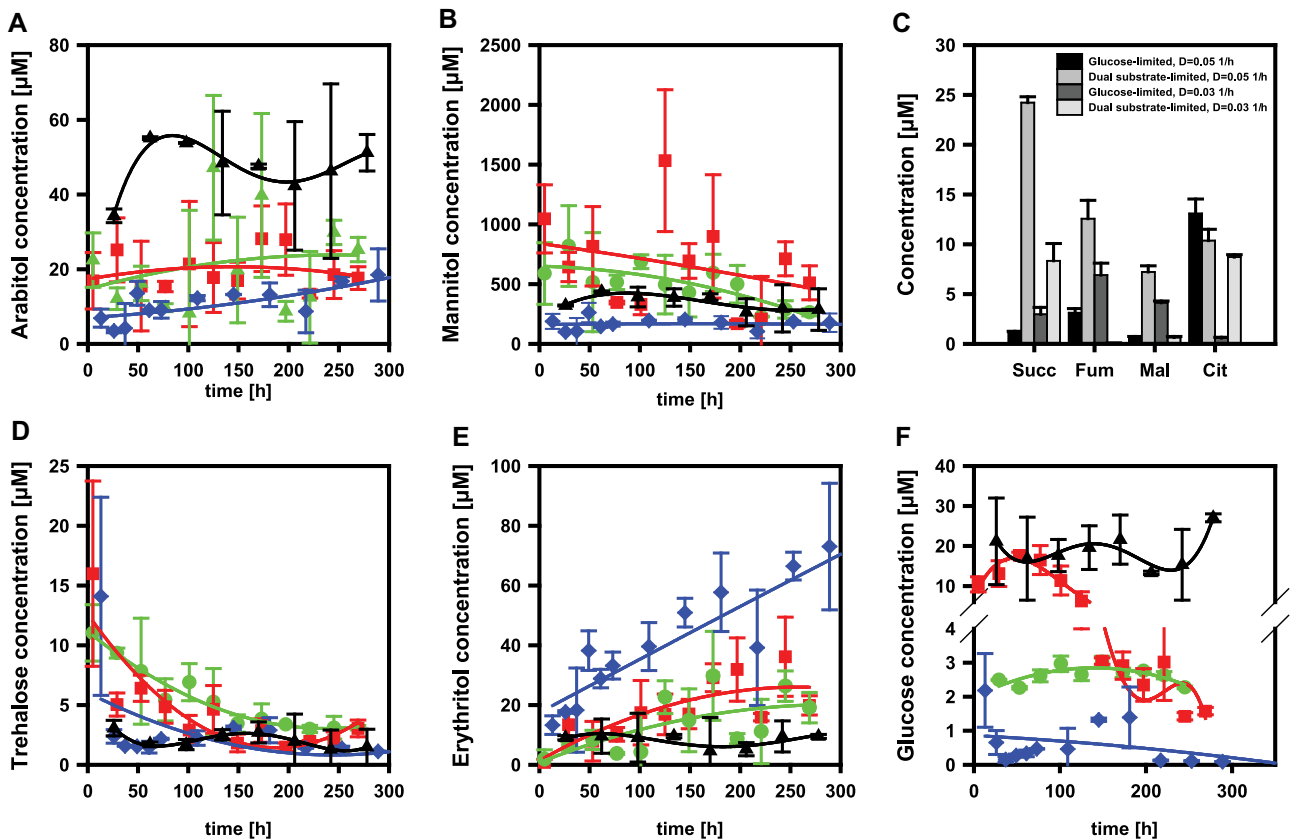


**Figure 5.** Extracellular metabolite concentrations of A) arabitol, B) mannitol, C) organic acids, D) trehalose, E) erythritol, and F) glucose. The glucose-limited chemostat culture (●, 0.05 h<sup>-1</sup>; ◆, 0.03 h<sup>-1</sup>); the dual substrate-limited chemostat culture (■, 0.05 h<sup>-1</sup>; ▲, 0.03 h<sup>-1</sup>). Measurements are given as the average ± standard deviation of at least three technical replicates. Time zero signifies the start-up of the chemostat cultivations. The solid curves show the trend lines of the experimental data within the observation time.

OPC, which cannot be recycled. Possibly, formate leads to lower levels of enzymes and/or enzyme activity with the OPC-forming branch pathway. However, the situation is just the opposite at  $D = 0.03 \text{ h}^{-1}$  (Figure 3A,B); therefore, more experiments should be carried out to confirm this hypothesis in the future.

### 3.3. Concentrations of Extra-/Intracellular Metabolites

It has been demonstrated by Hendrickx et al.<sup>[53]</sup> that Goeman's global test, which is used to determine whether a group of genes has a different expression pattern under changed conditions, can be generalized to metabolomics data for the determination of the behavior of a group of metabolites, belonging to the same pathway. In the previous section, we have shown that in the observed time range, there was a significant change in the flux distribution at  $D = 0.05 \text{ h}^{-1}$ , which did not occur at  $D = 0.03 \text{ h}^{-1}$ . In this study, Goeman's global test was used to determine whether a group of intracellular metabolites, such as intermediates in the glycolysis, the PP pathway, and the TCA cycle, were significantly different between the two carbon-limited chemostat conditions at  $D = 0.05 \text{ h}^{-1}$ . According to the result from Goeman's global test, compared with the glucose-limited chemostat culture, the dual substrate-limited chemostat culture showed significant changes in the metabolite levels of the central metabolic pathways, the levels in amino acids (except serine family and aromatic family), penicillin pathway-related metabolites, nucleotides, and storage carbohydrates (Table 2). Consistent with a significant change in the flux in the glycolytic pathway, Goeman's global test also indicated that there is a significant difference between the conditions. However, in contrast to the marginal difference regarding the flux distribution in the PP pathway between the two conditions, this result in turn suggests that under steady-state conditions, not all changes in the metabolic flux can be reflected in the metabolite level.

Another observation is that the intracellular glucose levels at the dilution rates of  $0.03 \text{ h}^{-1}$  and  $0.05 \text{ h}^{-1}$  are 1.5- and 3.7-fold higher, respectively, in the dual substrate-limited chemostat culture than in the glucose-limited chemostat condition (Figure 4B). This may also cause glucose repression as there might be an inverse relation between the intracellular glucose level and the penicillin production capacity under carbon-limited conditions.<sup>[42]</sup> At the same time, the cytosolic NADH/NAD<sup>+</sup> ratio, calculated as previously described using the C4 equilibrium pool (aspartate and malate) in the TCA cycle,<sup>[42]</sup> showed a declining redox state of the cytosol in the dual substrate-limited chemostat cultivation at  $D = 0.05 \text{ h}^{-1}$ , suggesting that the cells were gradually adapted to increase the regeneration of NAD<sup>+</sup> and thus the redox status; however, this ratio is three- to tenfold higher than that in the glucose-limited scenario. Furthermore, the higher redox status might be detrimental to the formation of sulfur-sulfur bonds in protein folding and/or functionality.<sup>[58]</sup> Our previous study also suggests that there might be an inverse relation between the redox status and penicillin productivity.<sup>[42]</sup> Consistent with this, the results at  $D = 0.03 \text{ h}^{-1}$  show that the higher  $q_{\text{PenG}}$  might benefit from the lower NADH/NAD<sup>+</sup> ratio (Figure 4A).

**Table 2.** Results of the score test for the *P. chrysogenum* metabolomics dataset when comparing the two carbon-limited conditions after 100 h (five residence times) of chemostat cultivation at a dilution rate of  $0.05 \text{ h}^{-1}$ .

Pathway	Metabolite	Q statistic	Not adjusted p-value	Bonferroni-adjusted p-value				
Central carbon metabolism								
Glycolysis	Glucose-6-phosphate	195	1.55e-04	<b>8e-05</b>				
	Fructose-6-phosphate							
	Mannose-6-phosphate							
	Mannitol-1-phosphate							
	Fructose-1,6-bisphosphate							
	2&3 Phosphoglycerate							
	Phosphoenolpyruvate							
	Pyruvate							
	PPP				6-Phosphogluconate	49	0.04	<b>0.04</b>
					Ribose-5-phosphate			
Ribulose-5-phosphate								
Sedoheptulose-7-phosphate								
TCA cycle	$\alpha$ -Ketoglutarate	157	1.20e-04	<b>1.55e-04</b>				
	Succinate							
	Fumarate							
	Malate							
	(i) Citric acid							
Amino acids biosynthesis								
Histidine family	Histidine	105	5.6e-03	<b>5.4e-03</b>				
	Cys							
Serine family	Serine	24	0.21	0.21				
	Glycine							
	Phenylalanine							
Aromatic family	Tyrosine	19	0.31	0.32				
	Alanine							
Pyruvate family	Val	75	5.5e-03	<b>5.3e-03</b>				
	Leucine							
	Aspartate							
Aspartate family	Asparagine	149	1.80e-04	<b>1.55e-04</b>				
	Methionine							
	Threonine							
	Isoleucine							
	Glutamate							
Glutamate family	Glutamine	117	3.6e-04	<b>3.1e-04</b>				
	Proline							
	$\alpha$ AAA							
	Lysine							
	PAA							
Other pathways								
Penicillin-related pathway	PAA	53	5e-03	<b>5e-03</b>				

(Continued)

**Table 2.** (Continued)

Pathway	Metabolite	Q statistic	Not adjusted p-value	Bonferroni-adjusted p-value
Nucleotides	PenG	64	2e−03	<b>2e−03</b>
	o-OH-PAA			
	6-APA			
	OPC			
	ATP			
	ADP			
Storage carbohydrates	AMP	113	1.2e−04	<b>1.6e−04</b>
	Arabitol			
	Erythritol			
	Mannitol			
	Trehalose			

Metabolites of the dataset together with their pathway assignments are listed. The permutation test is based on all permutations. Results are significant when the Bonferroni-adjusted  $p$ -value is smaller than 0.05. Significant results are indicated in bold.

Furthermore, the extracellular metabolite concentrations were shown (Figure 5). Under the two substrate-limited conditions at  $D = 0.05 \text{ h}^{-1}$ , extracellular arabitol concentration fluctuated, but seemed to remain within a value of about  $20 \mu\text{M}$ , while extracellular trehalose and mannitol concentrations decreased and erythritol concentrations increased throughout the cultivation process (Figure 5A,B,D). The changes in these storage carbohydrates followed the change in their intracellular counterparts (see Supporting Information). Although at  $D = 0.03 \text{ h}^{-1}$  the intracellular arabitol and mannitol levels are lower in the dual substrate-limited condition than in the glucose-limited condition, they are excreted more outside the cells (Figure 5A,B); in the dual substrate-limited condition extracellular arabitol and erythritol concentrations increased over time but they seem to remain invariably in the glucose-limited condition (Figure 5A,E). It can be observed from Figure 5C that at  $D = 0.05 \text{ h}^{-1}$ , extracellular organic acids including citric acid, succinic acid, fumaric acid, and malic acid are significantly excreted under the dual substrate-limited chemostat conditions. The higher accumulation of these organic acids in the culture medium constitutes evidence of restriction of the TCA cycle in which a large amount of NADH can be produced, likely caused by the higher NADH/NAD<sup>+</sup> ratio under the dual-substrate-limited conditions. This can be evidenced by the observation of a gradual increase in the flux through the TCA cycle, which is accompanied by the declining redox status in the dual substrate-limited conditions relative to the glucose-limited conditions (Figures 3C,D and 4A). In addition to this, the dysfunction of the TCA cycle may reverberate into upstream pathways producing overflow in the glycolytic pathway due to the limited consumption of pyruvate by the mitochondria: this might explain the increase in intracellular pyruvate, PEP, M1P, and other metabolites in

the glycolysis (see Supporting Information). To further verify the overflow in the glycolysis, in the ensuing experiment, analysis of extracellular metabolites should be broadly extended to primary metabolites in the central metabolic pathway.

Further, an interesting observation is that the extracellular glucose concentration ( $C_s$ ) at  $D = 0.05 \text{ h}^{-1}$  in the dual substrate-limited chemostat culture was higher during the first 75 h of chemostat cultivation and then gradually decreased to a very low value of about  $1.0 \mu\text{M}$  (Figure 5F). In the first phase (before 75 h), this could be caused by the gradual induction of FDH; in the second phase, FDH had already been fully induced and the residual formate concentration gradually decreased to a low and constant value (Figure 2). This observation is well consistent with the previous study by Harris et al.;<sup>[39]</sup> the NAD<sup>+</sup>-dependent FDH activity can only be induced by the formate in the feed and this activity increased linearly with the rate of formate consumption by the chemostat cultures. As a consequence, the cell may be adapted to consume more glucose rather than formate and this could be caused by the decreasing potential of passive uptake of formate and its incapability of being utilized for anabolic purposes. However, at  $D = 0.03 \text{ h}^{-1}$ , the  $C_s$  remained at a higher value of about  $18 \mu\text{M}$  in the dual substrate-limited condition than in the glucose-limited condition (Figure 5F). Together, the results in both conditions indicate that the higher  $q_{\text{PenG}}$  can benefit from steady  $C_s$ , while the low and decreasing  $C_s$  might be related to glucosensing and metabolic rearrangement.<sup>[42]</sup>

## 4. Conclusions

In glucose-limited chemostat cultures of the high-yielding *P. chrysogenum*, cofeeding of formate as the auxiliary substrate causes significant changes in metabolite levels, fluxomics, and penicillin productivity. In contrast with previous findings obtained at  $D = 0.03 \text{ h}^{-1}$ ,<sup>[39]</sup> no increases in biomass and penicillin yield on glucose were observed at  $D = 0.05 \text{ h}^{-1}$ . We concluded that these may be growth rate-related. The result showed that cofeeding of formate as the auxiliary substrate even gave rise to decreased penicillin productivity relative to the glucose-limited condition at the dilution rate of  $0.05 \text{ h}^{-1}$ . The test results by Goeman's global test indicated that there might not be a direct relation between the metabolite level and the metabolic flux pattern, for example in the PP pathway. Further, we observed that catabolism of formate at  $D = 0.05 \text{ h}^{-1}$  led to a higher cytosolic redox status and a higher intracellular glucose level, which may be especially detrimental to the biomass growth and penicillin productivity. The present work presents an example of the potential use and limitation of formate as the auxiliary substrate in penicillin production and helps to understand the impact of this dual substrate-limited condition on metabolite levels, fluxes, and penicillin productivity.

However, the results imply that the formate assimilation pathway in *P. chrysogenum* is far from ideal for biotechnological applications. More careful cell physiology studies and optimization strategies are fairly needed to ensure formate coassimilation to become a useful bioindustrial process. Typically, due to poor mixing and mass transfer limitations in an industrial practice, cells are therefore repeatedly exposed to

oscillating conditions, such as low/high substrate levels in different parts of the fermentor. This results in widely distributed specific substrate uptake rates ( $q_s$ ) and growth rates ( $\mu$ ) in the reactor.<sup>[16]</sup> Therefore, more relevant scale-down studies mimicking both inlet feed zone and the bulk zone farther away from the inlet feed zone should be carried out to confirm the potential of formate to be used as an auxiliary substrate in an industrial-scale scenario.

## Supporting Information

Supporting Information is available from the Wiley Online Library or from the author.

## Acknowledgements

The authors are very grateful to Dr. Diana M. Hendrickx for her assistance in Goeman's global test. This work was financially subsidized by the National Key Research and Development Program, 2017ZX7402003, Shanghai Municipal Natural Science Foundation (19ZR1413600), the NWO-MoST Joint Program, Grant number, 2013DFG32630, the 111 Project (B18022), and the Fundamental Research Funds for the Central Universities, 22221818014. The figure 4 was corrected on October, 1, 2019.

## Conflict of Interest

The authors declare no conflict of interest.

## Keywords

auxiliary substrates, chemostat, metabolomics, penicillin, *Penicillium chrysogenum*

Received: January 7, 2019

Revised: May 20, 2019

Published online: July 15, 2019

- [1] G. Ozcengiz, A. L. Demain, *Biotechnol. Adv.* **2013**, *31*, 287.
- [2] M. T. Prausse, S. Schauble, R. Guthke, S. Schuster, *Biotechnol. Bioeng.* **2016**, *113*, 173.
- [3] O. Fiehn, *Plant Mol. Biol.* **2002**, *48*, 155.
- [4] C. Jang, L. Chen, J. D. Rabinowitz, *Cell* **2018**, *173*, 822.
- [5] P. Song, K. Yuan, T. Qin, K. Zhang, X. J. Ji, L. Ren, R. Guan, J. Wen, H. Huang, *J. Ind. Microbiol. Biotechnol.* **2018**, *45*, 767.
- [6] M. Z. Ding, J. S. Cheng, W. H. Xiao, B. Qiao, Y. J. Yuan, *Metabolomics* **2009**, *5*, 229.
- [7] M. Mulleder, E. Calvani, M. T. Alam, R. K. Wang, F. Eckerstorfer, A. Zelezniak, M. Ralsler, *Cell* **2016**, *167*, 553e512.
- [8] Y. Guan, D. Yin, X. Du, X. Ye, *J. Ind. Microbiol. Biotechnol.* **2018**, *45*, 951.
- [9] X. Zheng, J. Yu, T. C. Cairns, L. Zhang, Z. Zhang, Q. Zhang, P. Zheng, J. Sun, Y. Ma, *Biotechnol. J.* **2019**, *14*, e1800315.
- [10] G. Wang, J. Zhao, X. Wang, T. Wang, Y. Zhuang, J. Chu, S. Zhang, H. J. Noorman, *Biochem. Eng. J.* **2019**, *146*, 41.
- [11] A. Kummel, S. Panke, M. Heinemann, *Mol. Syst. Biol.* **2006**, *2*, 00342006.
- [12] T. Cakir, K. R. Patil, Z. Onsan, K. O. Ulgen, B. Kirdar, J. Nielsen, *Mol. Syst. Biol.* **2006**, *2*, 50.
- [13] U. Nasution, W. M. van Gulik, C. Ras, A. Proell, J. J. Heijnen, *Metab. Eng.* **2008**, *10*, 10.
- [14] W. M. van Gulik, M. R. Antoniewicz, W. T. A. M. deLaat, J. L. Vinke, J. J. Heijnen, *Biotechnol. Bioeng.* **2001**, *72*, 185.
- [15] R. D. Douma, A. T. Deshmukh, L. P. de Jonge, B. W. de Jong, R. M. Seifar, J. J. Heijnen, W. M. van Gulik, *Biotechnol. Prog.* **2012**, *28*, 337.
- [16] C. Haringa, W. J. Tang, A. T. Deshmukh, J. Y. Xia, M. Reuss, J. J. Heijnen, R. F. Mudde, H. J. Noorman, *Eng. Life Sci.* **2016**, *16*, 652.
- [17] A. R. Lara, E. Galindo, O. T. Ramirez, L. A. Palomares, *Mol. Biotechnol.* **2006**, *34*, 355.
- [18] G. Wang, W. Tang, J. Xia, J. Chu, H. Noorman, W. M. van Gulik, *Eng. Life Sci.* **2015**, *15*, 20.
- [19] D. Molenaar, R. van Berlo, D. de Ridder, B. Teusink, *Mol. Syst. Biol.* **2009**, *5*, 323.
- [20] J. H. van Heerden, M. T. Wortel, F. J. Bruggeman, J. J. Heijnen, Y. J. Bollen, R. Planque, J. Hulshof, T. G. O'Toole, S. A. Wahl, B. Teusink, *Science* **2014**, *343*, 1245114.
- [21] L. P. de Jonge, N. A. Buijs, A. ten Pierick, A. Deshmukh, Z. Zhao, J. A. Kiel, J. J. Heijnen, W. M. van Gulik, *Biotechnol. J.* **2011**, *6*, 944.
- [22] G. Wang, J. Zhao, C. Haringa, W. Tang, J. Xia, J. Chu, Y. Zhuang, S. Zhang, A. T. Deshmukh, W. van Gulik, J. J. Heijnen, H. J. Noorman, *Microb. Biotechnol.* **2018**, *11*, 486.
- [23] W. Tang, A. T. Deshmukh, C. Haringa, G. Wang, W. van Gulik, W. van Winden, M. Reuss, J. J. Heijnen, J. Xia, J. Chu, H. J. Noorman, *Biotechnol. Bioeng.* **2017**, *114*, 1733.
- [24] C. Haringa, W. Tang, G. Wang, A. T. Deshmukh, W. A. van Winden, J. Chu, W. M. van Gulik, J. J. Heijnen, R. F. Mudde, H. J. Noorman, *Chem. Eng. Sci.* **2018**, *175*, 12.
- [25] W. M. van Gulik, W. T. de Laat, J. L. Vinke, J. J. Heijnen, *Biotechnol. Bioeng.* **2000**, *68*, 602.
- [26] W. Babel, *Eng. Life Sci.* **2009**, *9*, 285.
- [27] Z. Liu, T. Oyetunde, W. D. Hollinshead, A. Hermanns, Y. J. Tang, W. Liao, Y. Liu, *Biotechnol. Biofuels* **2017**, *10*, 22.
- [28] M. G. Kalyuzhnaya, A. W. Puri, M. E. Lidstrom, *Metab. Eng.* **2015**, *29*, 142.
- [29] H. Yu, J. C. Liao, *Nat. Commun.* **2018**, *9*, 3992.
- [30] J. Bang, S. Y. Lee, *Proc. Natl. Acad. Sci. U. S. A.* **2018**, *115*, E9271.
- [31] J. W. K. Oliver, S. Atsumi, *Metab. Eng.* **2015**, *29*, 106.
- [32] K. R. Choi, W. D. Jang, D. Yang, J. S. Cho, D. Park, S. Y. Lee, *Trends Biotechnol.* **2019**, <https://doi.org/10.1016/j.tibtech.2019.01.003>.
- [33] J. M. Clomburg, A. M. Crumbley, R. Gonzalez, *Science* **2017**, *355*, aag0804.
- [34] P. Durre, B. J. Eikmanns, *Curr. Opin. Biotechnol.* **2015**, *35*, 63.
- [35] O. Yishai, S. N. Lindner, J. Gonzalez de la Cruz, H. Tenenboim, A. Bar-Even, *Curr. Opin. Chem. Biol.* **2016**, *35*, 1.
- [36] S. J. Berrios-Rivera, G. N. Bennett, K. Y. San, *Metab. Eng.* **2002**, *4*, 217.
- [37] J. H. Ahn, J. Bang, W. J. Kim, S. Y. Lee, *Biotechnol. Bioeng.* **2017**, *114*, 2837.
- [38] J. M. Geertman, J. P. van Dijken, J. T. Pronk, *FEMS Yeast Res.* **2006**, *6*, 1193.
- [39] D. M. Harris, Z. A. van der Krogt, W. M. van Gulik, J. P. van Dijken, J. T. Pronk, *Appl. Environ. Microbiol.* **2007**, *73*, 5020.
- [40] U. Nasution, W. M. van Gulik, A. Proell, W. A. van Winden, J. J. Heijnen, *Metab. Eng.* **2006**, *8*, 395.
- [41] R. D. Douma, P. J. Verheijen, W. T. de Laat, J. J. Heijnen, W. M. van Gulik, *Biotechnol. Bioeng.* **2010**, *106*, 608.
- [42] G. Wang, B. Wu, J. Zhao, C. Haringa, J. Xia, J. Chu, Y. Zhuang, S. Zhang, J. J. Heijnen, W. van Gulik, A. T. Deshmukh, H. J. Noorman, *Biotechnol. Bioeng.* **2018**, *115*, 114.
- [43] M. R. Mashego, W. M. van Gulik, J. L. Vinke, J. J. Heijnen, *Biotechnol. Bioeng.* **2003**, *83*, 395.
- [44] R. M. Seifar, A. T. Deshmukh, J. J. Heijnen, W. M. van Gulik, *J. Sep. Sci.* **2012**, *35*, 225.

- [45] M. R. Mashego, L. Wu, J. C. Van Dam, C. Ras, J. L. Vinke, W. A. Van Winden, W. M. Van Gulik, J. J. Heijnen, *Biotechnol. Bioeng.* **2004**, *85*, 620.
- [46] L. Wu, M. R. Mashego, J. C. van Dam, A. M. Proell, J. L. Vinke, C. Ras, W. A. van Winden, W. M. van Gulik, J. J. Heijnen, *Anal. Biochem.* **2005**, *336*, 164.
- [47] G. Wang, J. Chu, Y. Zhuang, W. van Gulik, H. Noorman, *J. Biotechnol.* **2019**, *299*, 21.
- [48] C. Cipollina, A. ten Pierick, A. B. Canelas, R. M. Seifar, A. J. van Maris, J. C. van Dam, J. J. Heijnen, *J. Chromatogr. B: Anal. Technol. Biomed. Life Sci.* **2009**, *877*, 3231.
- [49] R. M. Seifar, C. Ras, J. C. van Dam, W. M. van Gulik, J. J. Heijnen, W. A. van Winden, *Anal. Biochem.* **2009**, *388*, 213.
- [50] R. M. Seifar, Z. Zhao, J. van Dam, W. van Winden, W. van Gulik, J. J. Heijnen, *J. Chromatogr. A* **2008**, *1187*, 103.
- [51] P.J. Verheijen, in *The Metabolic Pathway Engineering Handbook* (Ed: C.D. Smolke), CRC Press, Boca Raton, FL 2010, p. 8.1.
- [52] R. Agren, L. Liu, S. Shoaie, W. Vongsangnak, I. Nookaew, J. Nielsen, *PLoS Comput. Biol.* **2013**, *9*, e1002980.
- [53] D. M. Hendrickx, H. C. J. Hoefsloot, M. M. W. B. Hendriks, A. B. Canelas, A. K. Smilde, *Anal. Chim. Acta* **2012**, *719*, 8.
- [54] M. Rodriguez-Saiz, J. L. Barredo, M. A. Moreno, J. M. Fernandez-Canon, M. A. Penalva, B. Diez, *J. Bacteriol.* **2001**, *183*, 5465.
- [55] S. Wang, Y. Zhang, H. Dong, S. Mao, Y. Zhu, R. Wang, G. Luan, Y. Li, *Appl. Environ. Microbiol.* **2011**, *77*, 1674.
- [56] S. Grunwald, A. Mottet, E. Grousseau, J. K. Plassmeier, M. K. Popovic, J. L. Uribelarrea, N. Gorret, S. E. Guillouet, A. Sinskey, *Microb. Biotechnol.* **2015**, *8*, 155.
- [57] A. B. Canelas, W. M. van Gulik, J. J. Heijnen, *Biotechnol. Bioeng.* **2008**, *100*, 734.
- [58] N. M. Giles, A. B. Watts, G. I. Giles, F. H. Fry, J. A. Littlechild, C. Jacob, *Chem. Biol.* **2003**, *10*, 677.